



Solvent-deficient synthesis of nanocrystalline $\text{Ba}_{0.5}\text{Sr}_{0.5}\text{Co}_{0.8}\text{Fe}_{0.2}\text{O}_{3-\delta}$ powder

Saša Zeljković^{1,*}, Jin Miyawaki², Dragoljub Vranković³, Elena Tervoort⁴, Roland Hauert⁵, Toru Kotegawa⁶, Toni Ivas⁵

¹University of Banja Luka, Faculty of Natural Sciences and Mathematics, Department of Chemistry, Mladena Stojanovica 2, 78 000 Banja Luka, Bosnia and Herzegovina

²Kyushu University, Institute for Materials Chemistry and Engineering, 6-1 Kasugakoen, Kasuga, Fukuoka 816-8580, Japan

³Technische Universität Darmstadt, Jovanka-Bontschits Straße 2, 64287 Darmstadt, Germany

⁴ETH Zurich, Laboratory for Multifunctional Materials, Department of Materials, 8093 Zurich, Switzerland

⁵EMPA Dübendorf, Laboratory for Advanced Materials Processing, Ueberlandstrasse 129, 8600 Dübendorf, Switzerland

⁶Kyushu University, Interdisciplinary Graduate School of Engineering Science, 6-1 Kasugakoen, Kasuga, Fukuoka 816-8580, Japan

Received 28 May 2018; Received in revised form 12 September 2018; Accepted 15 November 2018

Abstract

Nanocrystalline $\text{Ba}_{0.5}\text{Sr}_{0.5}\text{Co}_{0.8}\text{Fe}_{0.2}\text{O}_{3-\delta}$ powders were prepared by a cost-effective solvent-deficient method using metal nitrates and ammonium bicarbonate as precursors. X-ray diffraction (XRD), specific surface determination (BET), thermal analyses (TG-DTA-DSC), dynamic light scattering (DLS) and scanning electron microscopy (SEM) were used to examine the effects of the calcination temperature on the $\text{Ba}_{0.5}\text{Sr}_{0.5}\text{Co}_{0.8}\text{Fe}_{0.2}\text{O}_{3-\delta}$ (BSCF) formation. XRD analysis showed that a cubic $\text{Ba}_{0.5}\text{Sr}_{0.5}\text{Co}_{0.8}\text{Fe}_{0.2}\text{O}_{3-\delta}$ was obtained after heating for 1 h at 1000 °C. BSCF nanocrystals with a diameter of about 25 nm were obtained. On the other hand, the sample mass was stabilized at 915 °C as recorded by thermogravimetric analysis (TG), indicating a formation of the complex BSCF oxide already at this temperature. The phase transformations during the synthesis of BSCF oxide are defined and confirmed with the note on the instability of the cubic phase. Using the four-point DC measurements between –73 °C and 127 °C, the band gap of 0.84 eV was determined. The solvent-deficient method used in this study to synthesize $\text{Ba}_{0.5}\text{Sr}_{0.5}\text{Co}_{0.8}\text{Fe}_{0.2}\text{O}_{3-\delta}$ showed distinct advantages in comparison with other synthesis techniques considering simplicity, rapid synthesis, and quality of the produced nanocrystals.

Keywords: $\text{Ba}_{0.5}\text{Sr}_{0.5}\text{Co}_{0.8}\text{Fe}_{0.2}\text{O}_{3-\delta}$, nanofabrication, calcination temperature

I. Introduction

The global demand for cheap, environmentally friendly and energy-efficient technologies has intensified research on the intermediate temperature solid oxide fuel cells (IT-SOFC) devices [1]. Cathode materials aimed for use in IT-SOFCs should possess high oxygen and electronic transport properties at intermediate temperatures (450–700 °C) and high compatibility with the

electrolyte material [1,2].

Currently, two dominant strategies to meet these requirements are: i) investigation of new chemical compositions [2] and ii) development or modification of preparative routes [3]. Among mixed ionic-electronic conducting oxides, $\text{Ba}_{0.5}\text{Sr}_{0.5}\text{Co}_{0.8}\text{Fe}_{0.2}\text{O}_{3-\delta}$ (BSCF) with a cubic perovskite structure has been shown to be one of the most promising materials [4]. BSCF is proposed as a new IT-SOFC cathode material [5,6] and an oxygen permeable membrane material [7]. After the first report by Shao *et al.* [8], the BSCF material was investigated for its preparation, phase struc-

*Corresponding authors: tel: +387 51 300 830,
e-mail: sasa.zeljkovic@pmf.unibl.org

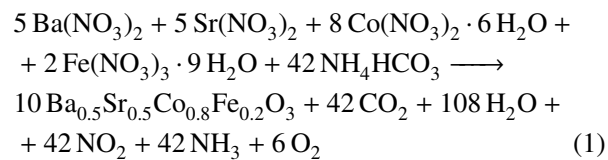
ture, thermal expansion coefficient and performance [9,10]. The observed BSCF chemical reaction with CO₂ [11,12] in the intermediate temperature ranges have limited the industrial application of BSCF. Regardless of these limitations, BSCF is still considered an interesting material as further research can enable routes to the thermochemically more stable materials [13].

Previously, BSCF has been prepared by several chemical methods including solid-state reaction synthesis [14], EDTA-citric acid complexing method [9], solution combustion synthesis [15], co-precipitation method [16], and by microwave-assisted synthesis [17]. Reducing the BSCF particle size proved to be highly desirable due to the good sintering properties and significantly enhanced oxygen reduction activity [18]. A recently reported solvent-deficient synthesis method [19] was used to produce very small (<5 nm) metal oxide nanoparticles such as Al₂O₃. The developed technique was reported to be unique in that a traditional solvent is not employed when mixing the reagents. The resulting “solvent-deficient” synthetic environment seems to cap particle growth, enabling a single procedure to yield a wide range of metal oxides nanoparticles without the use of capping agents [20]. During the mechanical mixing of metal nitrates hydrates and ammonium hydrogen carbonate, a chemical reaction occurs in the developed semiliquid environment. The ammonium nitrate forms in this slurry mixture, with partially or fully dissolved metallic cations. Continuous mixing with mortar and pestle causes mass transfer and helps to form the final product faster and easier in comparison with standard solid-state method where series of milling and heating steps are sometimes necessary to obtain final oxide in the single-phase form.

In this study, we investigate the structure and properties of BSCF nanoparticles produced by the solvent-deficient method as a function of the calcination temperature. Physicochemical characterizations have been conducted to verify the feasibility of the present route for nanocrystalline BSCF synthesis.

II. Experimental procedure

Ba_{0.5}Sr_{0.5}Co_{0.8}Fe_{0.2}O_{3-δ} (BSCF) nanocrystals were synthesized by a cost-effective solvent-deficient method using: Ba(NO₃)₂ (99%; Lachner, Czech Republic), Sr(NO₃)₂ (99+%, Acros, New Jersey, USA), Co(NO₃)₂ · 6 H₂O (98.0–102.0%, Carlo Erba Reagenti SpA), Fe(NO₃)₃ · 9 H₂O (99+%, Lachner, Czech Republic) and NH₄HCO₃ (99%, Acros, New Jersey, USA). All chemicals were used as received without further purification. Stoichiometrically calculated amounts of metal nitrates were ground together with ammonium bicarbonate for 20 min in mortar. The formed precursor slurry mixture was later annealed for 1 h at 500, 800 and 1000 °C. Heating was done in VIMS electric furnace at the rate of 10 °C/min. The final chemical reaction (Eq. 1) might be presented as follows:



Mixed solid precursors of BSCF, further used for thermal analysis, were pre-calcined for 1 h at 200 °C in air at the rate of 10 °C/min. Thermogravimetric/differential thermal analyses (TG/DTA) were carried out in the flowing air atmosphere (100 ml/min) with ca. 12 mg of the sample and with heating and cooling rates of 10 °C/min using EXSTAR TG/DTA6300 (Seiko Instruments Inc., Japan). The differential scanning calorimetry (DSC 404 F3 Pegasus, Netzsch, Selb Germany) analysis of the BSCF precursor was performed in a pure argon (PanGas, 99.9999% purity).

The phase identification of the samples was conducted with X-ray diffraction (XRD) on a PAN analytical X’Pert Powder XRD machine with Cu-K monochromator. Measurements were performed in the range from 20° to 100° of 2θ with 0.02° increments. The crystal structure of BSCF sample was obtained by Rietveld refinement using the Maud package [21]. The XRD experimental data were refined using lattice constants, zero offset, scale factors and full-width at half maximum as variable parameters. The structural parameters of the BSCF compound were obtained from the fitting results. The nanocrystalline size of the investigated samples was estimated using the Scherrer equation.

The particle size was obtained by dynamic light scattering (DLS) using Zetasizer Nano ZS (Malvern, UK). Before the measurement, samples were dispersed in water (dispersing agent) by using the ultrasonic processor UP200S (Hielscher-Ultrasound Technology) and subsequently transferred to the PMMA cuvette for measurement. Due to the unknown refractive index for measured samples, the reported values in this study are based on the light intensity and not on volume or numbers of particles.

Scanning electron microscopy (SEM) micrographs were recorded using a JOEL JSM-7600F Field Emission electron microscope. The acceleration voltage was 10 kV.

The X-ray photoelectron spectroscopy (XPS) was recorded on PHI Quantum 2000 (Physical Electronics Inc., Eden Prairie, MN) using an indium foil as a background layer and base pressure of 7.8 × 10⁻⁹ Torr. Both ionic and electronic neutralizers were running during the XPS measurements.

The Brunauer-Emmett-Teller (BET) specific surface area was determined from N₂ adsorption at –196 °C using a Quantachrome Autosorb iQ instrument. For these measurements, each sample was degassed at 200 °C for ~24 h to remove adsorbed moisture. The samples were allowed to equilibrate to room temperature before being cooled to –196 °C for data collection.

The powders were calcined at 1000 °C for 1 h and uniaxially pressed in pellets of 12 mm diameter and 3 mm thickness. The pellets were pressed with 440 MPa and then sintered at 1100 °C for 6 h. The density of sintered pellets was measured using standard Archimedes technique in ethanol using the Mettler-Toledo XS105 dual range balance. The low-temperature four-point DC measurements were done using Quantum Design Physical Property Measurement System (PPMS) between –73 and 127 °C. All measurements were repeated three times for reproducibility of the results.

III. Results and discussion

As previously mentioned, the mixture of precursors was pre-calcined at 200 °C for 1 h in the air. The TG/DTA experimental data of the pre-calcined BSCF precursor heated up to 1000 °C are shown in Figs. 1b and 1c together with the DSC data shown in Fig. 1a. Presented experiments revealed several endothermic and one strong exothermic peak. The complete synthesis consists out of four steps (A - endothermic weight loss, B - exothermic weight loss, C - endothermic weight loss, and D - endothermic weight loss). During the first step (A) a gradual endothermic weight loss up to 200 °C was observed, which was followed by the second step (B), marked by a sizeable exothermic peak and significant weight loss at 230 °C. Initial reactions during the mixing of the precursors at room temperature most probably included recombination and formation of

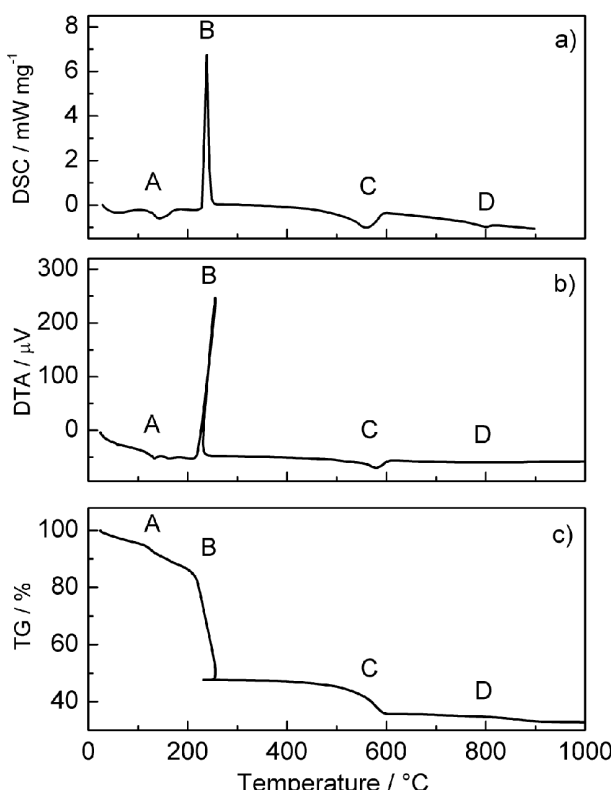
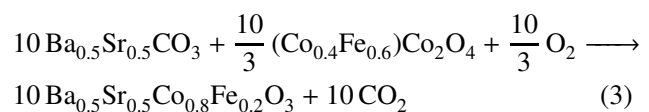
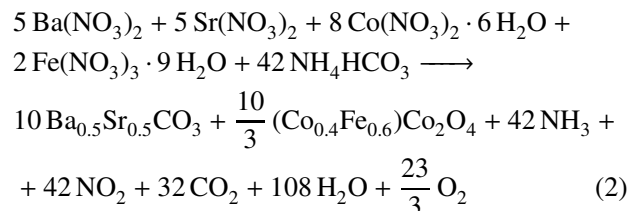


Figure 1. DSC (a), DTA (b) and TG (c) curves of pre-calcined BSCF precursor

NH_4NO_3 together with metallic cations bound in different compounds as mentioned in the study of nitrate reactions with ammonium bicarbonate [22]. Presumably, the intermediate compounds obtained after precursor mixing at room temperature included FeOOH , $\text{Co}(\text{OH})_2$, $\text{Co}_2(\text{OH})_3(\text{NO}_3)_2$ and $\text{Co}(\text{OH})(\text{NO}_3)_2 \cdot \text{H}_2\text{O}$, while barium and strontium intermediate compounds compositions are unclear. During preliminary heating to 200 °C, all intermediate compounds decomposed forming barium strontium carbonate and spinel (cobalt iron oxide) that can be represented by chemical Eq. 2. The TG recorded weight losses of the pre-calcined BSCF precursor at 200 and 230 °C are found to be 13.7 and 52.4%, respectively.

At temperatures over 500 °C barium strontium carbonate and Co-Fe spinel are transformed to finally produce hexagonal and cubic perovskite structure as presented in the chemical Eq. 3.



During the third step (C) an endothermic weight loss at around 580 °C was observed. Finally, at approximately 915 °C, there was an endothermic mass reduction (D).

An exothermic decomposition of NH_4NO_3 started at a temperature of about 230 °C [23]. The observed shifting of the large exothermic peak in the DTA signal was probably due to the intense heating of the sample in the air atmosphere. During the fierce exothermic reaction, DTA setup was not able to timely equilibrate and correct the temperature. Additional DSC experiment performed in a pure argon atmosphere as shown in Fig. 1a did not show the shifting of the peak, confirming that exothermic decomposition of the NH_4NO_3 in the air is very intense. As intermediate products, confirmed by XRD analysis (Figs. 2 and 3), there were $\text{Ba}_{0.5}\text{Sr}_{0.5}\text{CO}_3$ [24] and Fe-Co spinel [25]. The present $\text{Ba}_{0.5}\text{Sr}_{0.5}\text{CO}_3$ phase was gradually changed from aragonite to metastable form up to around 580 °C [12]. Around 580 °C, we can observe the gradual degradation of ar- $\text{Ba}_{0.5}\text{Sr}_{0.5}\text{CO}_3$ and intermediate $\text{Ba}_{0.5}\text{Sr}_{0.5}\text{Co}_{0.8}\text{Fe}_{0.2}\text{O}_{3-\delta}$ hexagonal phase formation. Starting from around 850 °C, there was substantial weight loss that can be related to the cubic BSCF phase formation.

Although the formation of cubic perovskite was to a large extent completed at about 915 °C, there was

a further slight decline in mass. This behaviour could be a consequence of the oxygen content change in the BSCF structure caused by increasing temperature [12], and hexagonal-cubic BSCF phase equilibrium [11]. The final overall recorded mass loss was ca. 68%.

The evolution of the phase composition from precursor into BSCF perovskite-type compounds during heating was followed by standard XRD measurements as shown in Fig. 2 and in-situ high-temperature XRD measurements as shown in Fig. 3. In Fig. 2, the XRD pattern of the powder heated at 500 °C indicated the formation of two types of Ba-Sr carbonates: ar-orthorhombic aragonite-type carbonate, $\text{Ba}_{0.5}\text{Sr}_{0.5}\text{CO}_3$, and δ -metastable monoclinic carbonate, $\text{Ba}_{0.5}\text{Sr}_{0.5}\text{CO}_3$ [24]. At 800 °C, $\delta\text{-Ba}_{0.5}\text{Sr}_{0.5}\text{CO}_3$ converted completely to ar- $\text{Ba}_{0.5}\text{Sr}_{0.5}\text{CO}_3$. In the powder annealed at 1000 °C, the carbonates were no longer present. The XRD pattern of the sample heated at 800 °C was indicative because two phases of BSCF, namely P-BSCF cubic phase and P1-BSCF intermediate hexagonal phase, are present. P1 hexagonal phase is present also after thermal treatment at 1000 °C. The part of the single cubic P-BSCF phase transformed upon slow cooling between 900 °C and 700 °C to a mixture of cubic and hexagonal phases.

High-temperature XRD measurements shown in Fig. 3 reveal that $\text{Ba}_{0.5}\text{Sr}_{0.5}\text{CO}_3$ (in aragonite and metastable forms) and Co-Fe spinel phases were formed already at 200 °C and were thermodynamically stable up to 600 °C where intermediate BSCF hexagonal phase was formed. The hexagonal BSCF phase disappeared after 900 °C contrary to previous measurements (Fig. 2) where it was still present even after heating at 1000 °C. This difference in obtained data is probably caused by an absence of isothermal steps and insufficient time for the hexagonal to a cubic phase transition.

The appearance of the $\text{Ba}_{1-x}\text{Sr}_x\text{Co}_{2-y}\text{Fe}_y\text{O}_{5-\delta}$ lamellar phase with the XRD peak at 30.5° required further inspection of the BSCF cubic phase stability and was the reason for the BSCF phase stability follow-up experiment. The starting material was this time heated at 1000 °C for 72 h and compared using XRD with material heated at the same temperature for 1 h. The results are shown in Fig. 4 and they confirm that after 72 h at 1000 °C the cubic BSCF phase (P) deteriorates into hexagonal BSCF phase (P1) and $\text{Ba}_{1-x}\text{Sr}_x\text{Co}_{2-y}\text{Fe}_y\text{O}_{5-\delta}$ phase (P2). It is important to note that the $\text{Ba}_{1-x}\text{Sr}_x\text{Co}_{2-y}\text{Fe}_y\text{O}_{5-\delta}$ phase (denoted as P2) was present but unmarked in previous papers that examined BSCF phase stability [11]. This result represented further evidence of the thermodynamic instability of the cubic BSCF phase. There is still discussion in the literature about the stability and the decomposition path of the cubic BSCF phase. Mueller *et al.* [11] have suggested that $\text{Ba}_{0.5}\text{Sr}_{0.5}\text{Co}_{0.8}\text{Fe}_{0.2}\text{O}_{3-\delta}$ composition lays in the miscibility gap and decomposes to hexagonal $\text{BaCoO}_{3-\delta}$ and cubic $\text{SrFeO}_{3-\delta}$ perovskite structures. Although the BSCF diffraction patterns indicate the existence of phase P2 annealed at 900 °C for four days, these

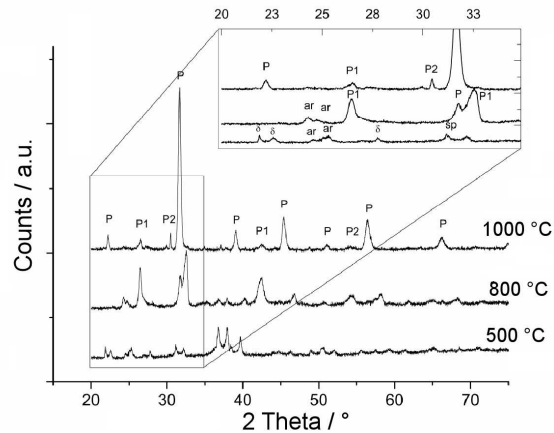


Figure 2. Evolution of the phase composition of the powder prepared by solvent-deficient method with marked peaks of: P-BSCF cubic, P1-BSCF hexagonal, P2-BSCF lamellar, ar- $\text{Ba}_{0.5}\text{Sr}_{0.5}\text{CO}_3$, $\delta\text{-Ba}_{0.5}\text{Sr}_{0.5}\text{CO}_3$ and sp-Co-Fe spinel

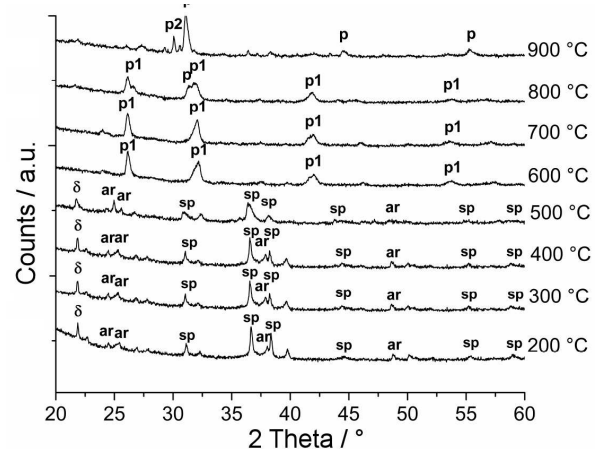


Figure 3. High-temperature XRD measurements in the range from 200 to 900 °C with marked peaks of: P-BSCF cubic, P1-BSCF hexagonal, P2-BSCF lamellar, ar- $\text{Ba}_{0.5}\text{Sr}_{0.5}\text{CO}_3$, $\delta\text{-Ba}_{0.5}\text{Sr}_{0.5}\text{CO}_3$ and sp-Co-Fe spinel

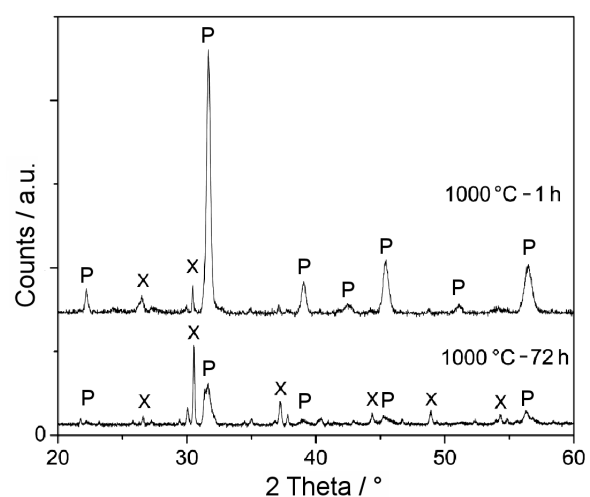


Figure 4. The XRD pattern of the powder annealed at 1000 °C for 1 h shows deterioration of the of P-BSCF cubic phase into P1-BSCF hexagonal phase and P2-BSCF lamellar (both marked with X) phase after annealing for 72 h

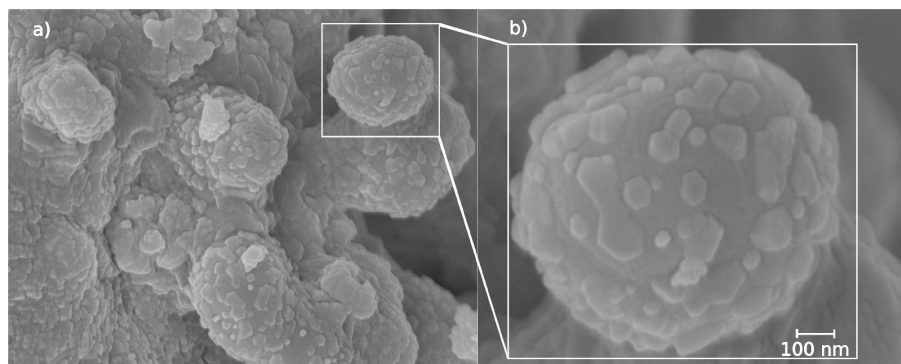


Figure 5. SEM image of the BSCF powder annealed at 1000 °C a) microstructure of the BSCF powder b) close-up of the microstructure showing aggregation of the hexagonal nanocrystals in larger agglomerates

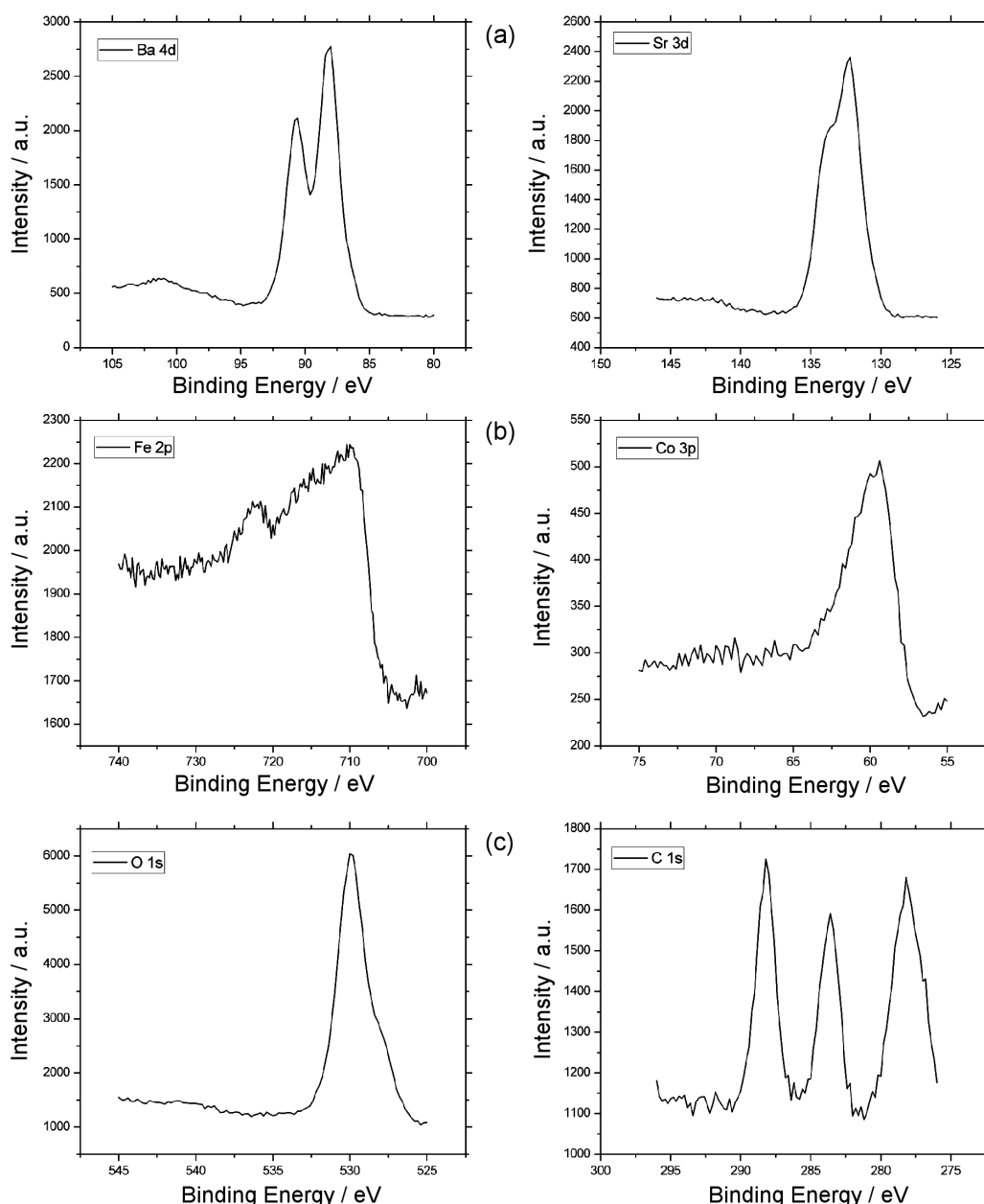


Figure 6. XPS spectra of the BSCF material produced by the solvent-deficient method after annealing for 1h at 1000 °C: a) A-site elements in the perovskite structure, b) B-site elements in the perovskite structure and c) O 1s and C 1s spectra of the BSCF material

authors did not discuss the existence of this phase further in their study. The perovskite decomposition study at intermediate temperatures by tunnelling electron microscopy was studied by Efimov *et al.* [26]. These authors observed an unknown lamellar structure with composition $\text{Ba}_{1-x}\text{Sr}_x\text{Co}_{2-y}\text{Fe}_y\text{O}_{5-\delta}$. This new phase is related to $15\text{R} \text{ SrMn}_{1-x}\text{Fe}_x\text{O}_{3-\delta}$ with the $(\text{cchch})_3$ stacking sequence [27].

The calculated intensities of the cubic perovskite and lamellar $\text{Ba}_{1-x}\text{Sr}_x\text{Co}_{2-y}\text{Fe}_y\text{O}_{5-\delta}$ compare well with XRD patterns. Thus, we conclude that the $\text{Ba}_{0.5}\text{Sr}_{0.5}\text{Co}_{0.8}\text{Fe}_{0.2}\text{O}_{3-\delta}$ phase decomposed to hexagonal perovskite, lamellar $\text{Ba}_{1-x}\text{Sr}_x\text{Co}_{2-y}\text{Fe}_y\text{O}_{5-\delta}$, and $\text{Ba}_{0.4}\text{Sr}_{0.6}\text{O}$ [26], but the exact decomposition path of the cubic BSCF is still questionable. The driving force for the BSCF decomposition should be a change of the cobalt valence state coupled with spin-state transitions of the cobalt ions in the perovskite structure [28–30]. The decomposition of cubic BSCF phase to hexagonal phase is slower in ceramic bulk material than in the powders [11]. Owing to the significant increase of the intensities of $\text{Ba}_{1-x}\text{Sr}_x\text{Co}_{2-y}\text{Fe}_y\text{O}_{5-\delta}$ peaks in our study in contrast to similar micro-sized powders investigated previously [11] we can conclude that the nanocrystalline powders preferentially decompose into the lamellar structure.

The SEM analysis of the powder annealed at 1000 °C revealed the structure and size of the grains as shown in Fig. 5. Overall structure consists of smaller hexagonal shaped polycrystals forming larger agglomerates. The hexagonal shaped crystals are plate-like in form and dimensions correspond to results obtained by the Scherrer's method. However, during annealing at higher temperatures, the polycrystals sinter in larger globular agglomerates as shown in Fig. 5b.

The BSCF surface composition is investigated using XPS. Figure 6 shows the corresponding XPS spectra of the BSCF surface. The peaks used for the element quantification are Ba 4d, Co 3p, Fe 2p, Sr 3d, O 1s, and C 1s. The relative concentrations of the elements are Sr 33.75%, Ba 32.9%, Co 25%, and Fe 8.33%. The charging compensation by shifting the low energy peak of C 1s 284.8 eV results from the presence of adventitious carbon, which is due to the atmospheric contamination. The peak at higher energy (289.0 eV) is due to the carbonates [31], and previous studies suggested it is due to the thermal treatment in static air. The Ba 4d peak is spin-orbital split. The Co 2p_{1/2} and 2p_{3/2} are overlapping with the Ba 3d_{3/2} and 3d_{5/2}. The Sr 3d peaks shown in Fig. 6 have a 2 eV orbital split (doublet). The main peaks of Sr 3d doublet are located at 133.7 eV and 132.6 eV, respectively. Similar values have been measured in perovskite structures [32]. Moreover, we can assign a doublet to the Sr²⁺ cation in the perovskite structure. Fe 2p signal overlaps with the Co Auger peak, and it is characteristic for several Fe-oxide compounds. The O 1s has peak at 529.0 eV and the main peak at 531.1 eV. The strongest peak at 531.1 eV is related to the

adsorbed oxygen species and carbonates [33,34], while the peak at 529.0 eV corresponds to the coordination of the B site Co, and Fe [35].

The agglomerate size distribution of the powders heated at different temperatures obtained from the DLS analysis is shown in Fig. 7. The agglomerate size decreases with increasing calcination temperature. The agglomerate size of the BSCF powder, calcined at 1000 °C was measured to be around 300 nm. Such a large grain size contradicts results obtained by XRD analysis. The observed difference is probably caused by the aggregation of nanocrystals into larger agglomerates.

The nitrogen adsorption experiments conducted on all the investigated BSCF powders revealed a low specific surface area, i.e.: 9.5, 15.0, 1.5 and 0.8 m²/g for BSCF powders calcined at 500, 600, 800 and 1000 °C, respectively. As mentioned previously, such a low specific surface area is a consequence of the nanocrystalline agglomeration into larger grains. The general trend of the temperature-induced decrease in a specific surface area correlated well with agglomerate size distribution.

The density of the BSCF sample sintered at 1100 °C for 6 h is measured to be 5.0 g/cm³. Thus, the relative density of BSCF sample is approx. 91% TD. The electrical resistance of the sintered BSCF sample as a function of the temperature is presented in Fig. 8. By using well-known relation for the resistivity of the semiconductor materials:

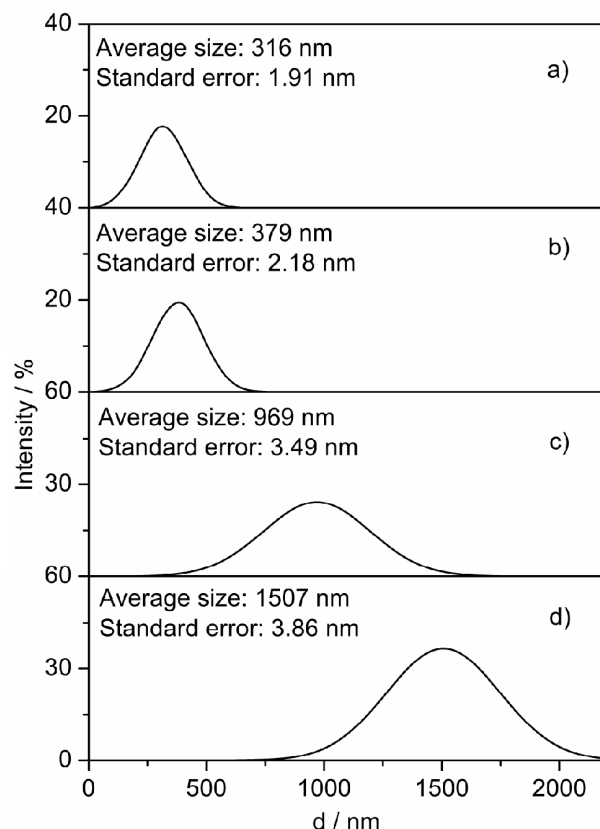


Figure 7. The agglomerate size distribution (DLS analysis) of the powders prepared by the solvent-deficient method and calcined at: a) 1000, b) 800, c) 600 and d) 500 °C

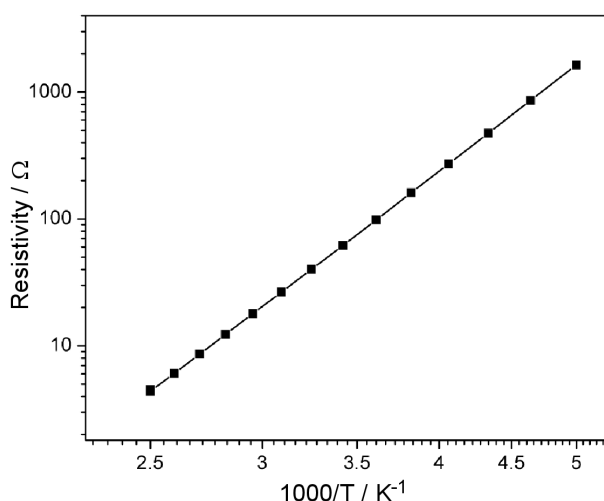


Figure 8. Resistance of the BSCF sample measured between 200 K and 400 K (the squares are measured values, and the line represents fit to the measured data)

$$\rho = A \cdot \exp \frac{E_g}{2k \cdot T} \quad (4)$$

where E_g is band gap, T is temperature, and k is Boltzmann constant, we calculated the band-gap value of 0.84 eV.

IV. Conclusions

A novel solvent-deficient method previously used for the synthesis of binary oxides was in this work applied for the rapid and simple preparation of nanocrystalline $Ba_{0.5}Sr_{0.5}Co_{0.8}Fe_{0.2}O_{3-\delta}$. The BSCF powder forms mainly the cubic form after calcination at 1000 °C for 1 h. Evolution of the phase composition of the BSCF prepared by the solvent-deficient method included nitrates and ammonium-bicarbonate reaction and decomposition, followed by the formation of intermediate aragonite $Ba_{0.5}Sr_{0.5}CO_3$, δ -metastable $Ba_{0.5}Sr_{0.5}CO_3$ and Co-Fe spinel phases. At around 600 °C the formation of intermediate BSCF hexagonal phase was observed, which transformed to cubic BSCF phase above 900 °C. The cubic BSCF phase deteriorates during prolonged annealing at 1000 °C as observed by high-temperature XRD measurement. The nanocrystalline powder investigated in our study decomposes preferentially to hexagonal perovskite, lamellar $Ba_{1-x}Sr_xCo_{2-y}Fe_yO_{5-\delta}$ oxide, and $Ba_{0.4}Sr_{0.6}O$.

The XRD analysis indicated that the produced BSCF phase has a nanocrystalline size of 20 to 25 nm. The particle size distribution is one order of magnitude higher due to the aggregation of nanocrystals into much larger agglomerates and was measured to be around 300 nm. The agglomeration of nanocrystals was confirmed by SEM study and subsequently with nitrogen adsorption experiments. The XPS measurements of the powder revealed the presence of adventitious carbon due to the atmospheric contamination. The relative atomic com-

positions of Sr 33.75%, Ba 32.9%, Co 25%, and Fe 8.33% were measured in samples annealed at 1000 °C. The four-point DC measurements of the final powder revealed semiconductor behaviour of the BSCF material at low temperatures. The band-gap obtained from these measurements is 0.84 eV.

In conclusion, our study provides a new synthesis method for the nanocrystalline complex oxide perovskites. The $Ba_{0.5}Sr_{0.5}Co_{0.8}Fe_{0.2}O_{3-\delta}$ perovskite investigated here raises new questions of the nanoparticle phase stability that will be addressed in future work.

Acknowledgement: This work was supported by the Ministry of Science and Technology of Republic of Srpska (grant number 19/6-020/961-49/12).

References

- D.J.L. Brett, A. Atkinson, N.P. Brandon, S.J. Skinner, "Intermediate temperature solid oxide fuel cells", *Chem. Soc. Rev.*, **37** (2008) 1568–1578.
- A. Tarancón, M. Burriel, J. Santiso, S.J. Skinner, J.A. Kilkner, "Advances in layered oxide cathodes for intermediate temperature solid oxide fuel cells", *J. Mater. Chem.*, **20** (2010) 3799–3813.
- J.H. Kim, Y.M. Park, H. Kim, "Nano-structured cathodes based on $La_{0.6}Sr_{0.4}Co_{0.2}Fe_{0.8}O_{3-\delta}$ for solid oxide fuel cells", *J. Power Sources*, **196** (2011) 3544–3547.
- J. Richter, P. Holtappels, T. Graule, T. Nakamura, L.J. Gauckler, "Materials design for perovskite SOFC cathodes", *Monatsh. Chem.*, **140** (2009) 985–999.
- C.K. Dyer, "Fuel cells for portable applications", *J. Power Sources*, **106** (2002) 31–34.
- F. Schulze-Küppers, S. Baumann, W.A. Meulenberg, D. Stöver, H.-P. Buchkremer, "Manufacturing and performance of advanced supported $Ba_{0.5}Sr_{0.5}Co_{0.8}Fe_{0.2}O_{3-\delta}$ (BSCF) oxygen transport membranes", *J. Membr. Sci.*, **433** (2013) 121–125.
- H. Wang, C. Tablet, A. Feldhoff, J. Caro, "Investigation of phase structure, sintering, and permeability of perovskite-type $Ba_{0.5}Sr_{0.5}Co_{0.8}Fe_{0.2}O_{3-\delta}$ membranes", *J. Membr. Sci.*, **262** (2005) 20–26.
- Z. Shao, S.M. Haile, "A high-performance cathode for the next generation of solid-oxide fuel cells", *Nature*, **431** (2004) 170–173.
- J. Martynczuk, M. Arnold, H. Wang, J. Caro, A. Feldhoff, "How $(Ba_{0.5}Sr_{0.5})(Fe_{0.8}Zn_{0.2})O_{3-\delta}$ and $(Ba_{0.5}Sr_{0.5})(Co_{0.8}Fe_{0.2})O_{3-\delta}$ perovskites form via an EDTA/citric acid complexing method", *Adv. Mater.*, **19** (2007) 2134–2140.
- M. Arnold, H. Wang, A. Feldhoff, "Influence of CO_2 on the oxygen permeation performance and the microstructure of perovskite-type $(Ba_{0.5}Sr_{0.5})(Co_{0.8}Fe_{0.2})O_{3-\delta}$ membranes", *J. Membr. Sci.*, **293** (2007) 44–52.
- D.N. Mueller, R.A. De Souza, T.E. Weirich, D. Roehrens, J. Mayer, M. Martin, "A kinetic study of the decomposition of the cubic perovskite-type oxide $Ba_xSr_{1-x}Co_{0.8}Fe_{0.2}O_{3-\delta}$ (BSCF) ($x = 0.1$ and 0.5)", *Phys. Chem. Chem. Phys.*, **12** (2010) 10320.
- S. Zeljković, T. Ivas, S. Vaucher, D. Jelić, L.J. Gauckler, "The changes of $Ba_{0.5}Sr_{0.5}Co_{0.8}Fe_{0.2}O_{3-\delta}$ perovskite oxide on heating in oxygen and carbon dioxide atmospheres", *J. Serb. Chem. Soc.*, **79** (2014) 1141–1154.

13. E.A. Kotomin, Y.A. Mastrikov, M.M. Kuklja, R. Merkle, A. Roytburd, J. Maier, “First principles calculations of oxygen vacancy formation and migration in mixed conducting $\text{Ba}_{0.5}\text{Sr}_{0.5}\text{Co}_{1-y}\text{Fe}_y\text{O}_{3-\delta}$ perovskites”, *Solid State Ionics*, **188** (2011) 1–5.
14. L. Tan, X. Gu, L. Yang, W. Jin, L. Zhang, N. Xu, “Influence of powder synthesis methods on microstructure and oxygen permeation performance of $\text{Ba}_{0.5}\text{Sr}_{0.5}\text{Co}_{0.8}\text{Fe}_{0.2}\text{O}_{3-\delta}$ perovskite-type membranes”, *J. Membr. Sci.*, **212** (2003) 157–165.
15. B. Liu, Y. Zhang, “ $\text{Ba}_{0.5}\text{Sr}_{0.5}\text{Co}_{0.8}\text{Fe}_{0.2}\text{O}_3$ nanopowders prepared by glycine-nitrate process for solid oxide fuel cell cathode”, *J. Alloys Compd.*, **453** (2008) 418–422.
16. M.S. Toprak, M. Darab, G.E. Syvertsen, M. Muhammed, “Synthesis of nanostructured BSCF by oxalate co-precipitation - As potential cathode material for solid oxide fuel cells”, *Int. J. Hydrog. Energy*, **35** (2010) 9448–9454.
17. S. Zeljković, J. Penavin-Škundrić, T. Ivas, S. Vaucher, “Synthesis of $\text{Ba}_{0.5}\text{Sr}_{0.5}\text{Co}_{0.8}\text{Fe}_{0.2}\text{O}_{3-\delta}$ from different precursor materials employing microwave heating”, *Contemp. Mater.*, **1** (2010) 61–67.
18. C. Su, X. Xu, Y. Chen, Y. Liu, M.O. Tadé, Z. Shao, “A top-down strategy for the synthesis of mesoporous $\text{Ba}_{0.5}\text{Sr}_{0.5}\text{Co}_{0.8}\text{Fe}_{0.2}\text{O}_{3-\delta}$ as a cathode precursor for buffer layer-free deposition on stabilized zirconia electrolyte with a superior electrochemical performance”, *J. Power Sources*, **274** (2015) 1024–1033.
19. B.F. Woodfield, S. Liu, J. Boerio-Goates, Q. Liu, S.J. Smith, “Preparation of uniform nanoparticles of ultra-high purity metal oxides, mixed metal oxides, metals, and metal alloys”, *US Patent 8211388*, 2012.
20. S.J. Smith, S. Amin, B.F. Woodfield, J. Boerio-Goates, B.J. Campbell, “Phase progression of $\gamma\text{-Al}_2\text{O}_3$ nanoparticles synthesized in a solvent-deficient environment”, *Inorg. Chem.*, **52** (2013) 4411–4423.
21. L. Lutterotti, “Total pattern fitting for the combined size-strain-stress-texture determination in thin film diffraction”, *Nucl. Instrum. Meth. B*, **268** (2010) 334–340.
22. S.J. Smith, B. Huang, S. Liu, Q. Liu, R.E. Olsen, J. Boerio-Goates, B.F. Woodfield, “Synthesis of metal oxide nanoparticles via a robust “solvent-deficient” method”, *Nanoscale*, **7** (2015) 144–156.
23. Y. Izato, A. Miyake, “Thermal decomposition mechanism of ammonium nitrate and potassium chloride mixtures”, *J. Therm. Anal. Calorim.*, **121** (2015) 287–294.
24. F. Deganello, L.F. Liotta, G. Marci, E. Fabbri, E. Traversa, “Strontium and iron-doped barium cobaltite prepared by solution combustion synthesis: exploring a mixed-fuel approach for tailored intermediate temperature solid oxide fuel cell cathode materials”, *Mater. Renew. Sustain. Energy*, **2** (2013) 8.
25. M. Vadivel, R.R. Babu, K. Ramamurthi, M. Arivanandhan, “Enhanced dielectric and magnetic properties of polystyrene added CoFe_2O_4 magnetic nanoparticles”, *J. Phys. Chem. Solids*, **102** (2017) 1–11.
26. K. Efimov, Q. Xu, A. Feldhoff, “Transmission electron microscopy study of $\text{Ba}_{0.5}\text{Sr}_{0.5}\text{Co}_{0.8}\text{Fe}_{0.2}\text{O}_{3-\delta}$ perovskite decomposition at intermediate temperatures”, *Chem. Mater.*, **22** (2010) 5866–5875.
27. E.J. Cussen, J. Sloan, J.F. Vente, P.D. Battle, T.C. Gibb, “ $15\text{R SrMn}_{1-x}\text{Fe}_x\text{O}_{3-\delta}$ ($x \approx 0.1$): a new perovskite stacking sequence”, *Inorg. Chem.*, **37** (1998) 6071–6077.
28. M. Arnold, T.M. Gesing, J. Martynczuk, A. Feldhoff, “Correlation of the formation and the decomposition process of the BSCF perovskite at intermediate temperatures”, *Chem. Mater.*, **20** (2008) 5851–5858.
29. A.S. Harvey, Z. Yang, A. Infortuna, D. Beckel, J.A. Purton, L.J. Gauckler, “Development of electron holes across the temperature-induced semiconductor-metal transition in $\text{Ba}_{1-x}\text{Sr}_x\text{Co}_{1-y}\text{Fe}_y\text{O}_{3-\delta}$ ($x, y = 0.2–0.8$): A soft X-ray absorption spectroscopy study”, *J. Phys. Condens. Matter*, **21** (2009) 015801.
30. A.S. Harvey, F.J. Litterst, Z. Yang, J.L.M. Rupp, A. Infortuna, L.J. Gauckler, “Oxidation states of Co and Fe in $\text{Ba}_{1-x}\text{Sr}_x\text{Co}_{1-y}\text{Fe}_y\text{O}_{3-\delta}$ ($x, y = 0.2–0.8$) and oxygen desorption in the temperature range 300–1273 K”, *Phys. Chem. Chem. Phys.*, **11** (2009) 3090–3098.
31. N.H. Batis, P. Delichere, H. Batis, “Physicochemical and catalytic properties in methane combustion of $\text{La}_{1-x}\text{Ca}_x\text{MnO}_{3\pm y}$ ($0 \leq x \leq 1$; $-0.04 \leq y \leq 0.24$) perovskite-type oxide”, *Appl. Catal. A Gen.*, **282** (2005) 173–180.
32. P. Wang, L. Yao, M. Wang, W. Wu, “XPS and voltammetric studies on $\text{La}_{1-x}\text{Sr}_x\text{CoO}_{3-\delta}$ perovskite oxide electrodes”, *J. Alloys Compd.*, **311** (2000) 53–56.
33. S. Petrović, L. Karanović, P.K. Stefanov, M. Zdujić, A. Terlecki-Baričević, “Catalytic combustion of methane over Pd containing perovskite type oxides”, *Appl. Catal. B Environ.*, **58** (2005) 133–141.
34. D. Fino, N. Russo, E. Cauda, G. Saracco, V. Specchia, “La-Li-Cr perovskite catalysts for diesel particulate combustion”, *Catal. Today*, **114** (2006) 31–39.
35. J.F. Moulder, W.F. Stickle, P.E. Sobol, K.D. Bomben, *Handbook of X-ray Photoelectron Spectroscopy: A Reference Book of Standard Spectra for Identification and Interpretation of XPS Data*, Ed. J. Chastain, R.C. King Jr., Physical Electronics, USA, 1995.